J Vis (2013) 16:145–151
DOI 10.1007/s12650-013-0157-2

REGULAR PAPER

V. V. Korolev · I. G. Kovalenko

# A rate-of-strain-based method of hydrodynamic flow analysis: identification of discontinuities, compression–rarefaction and shear waves

Received: 13 February 2012 / Revised: 23 December 2012 / Accepted: 22 January 2013 / Published online: 15 February 2013


**Abstract** We present an original method for recognition of different types of hydrodynamic discontinuities such as shock fronts and tangential discontinuities, smooth types of flows such as rarefaction waves, and their intensities simultaneously. The method is based on invariants of a strain velocity tensor of hydrodynamic flow. We demonstrate the advantages of this new technique by way of giving an example of a supersonic turbulence produced by a blast wave from a point explosion propagating in a 'cloudy' inhomogeneous medium.

**Keywords** Hydrodynamic discontinuities · Shock waves · Turbulence · Flow visualization

## 1 Introduction

Hydrodynamic flow analysis often requires detection of a shock-wave or other types of discontinuities. There are many methods of discontinuity detection, as a rule, each one oriented at recognition of a specific type of jumps (Vorozhtsov and Yanenko 1980). In ordinary cases calculation of velocity divergence, vorticity or schlieren map is sufficient.

Complex flows such as turbulent flows, and especially supersonic turbulent flows require simultaneous detection, recognition, and tracking numerous discontinuities. In such a case localization of jumps and their identification require a more delicate and precise technique. This poses a challenge of developing an easy-to-use universal arbitrary-jump-capturing technique applicable to all types of flow.

In the present paper we propose an original advanced method of recognizing, apart from different types of hydrodynamic discontinuities, smooth types of flows such as rarefaction waves, and their intensities simultaneously.

Supported by the RFBR grants 11-02-01332a, 11-02-97124r_povolzhie_a and by the State agreement 14.B37.21.0915 of the Russian Ministry of Education and Research.

**Electronic supplementary material** The online version of this article (doi:10.1007/s12650-013-0157-2) contains supplementary material, which is available to authorized users.

V. V. Korolev · I. G. Kovalenko (✉)
Physicotechnical Institute, Volgograd State University, Volgograd 400062, Russia
E-mail: ilya.g.kovalenko@gmail.com

V. V. Korolev
E-mail: vitokorolev@gmail.com

## 2 The method

Given the velocity vector field $\mathbf{v}(\mathbf{x})$, recognition of subdomains of qualitatively different types of flow such as jumps or smooth compression/expansion or shear is required.

Locally, the flow field is characterized by the velocity gradient tensor $\partial v_i/\partial x_j$ which can be decomposed into the antisymmetric part (vorticity) and the symmetric part (the strain velocity tensor)

$$D_{ij} = \frac{1}{2}\left(\frac{\partial v_i}{\partial x_j} + \frac{\partial v_j}{\partial x_i}\right), \quad i,j = \overline{1,3}. \tag{1}$$

We postulate the coordinate independence of the method; this implies that recognition should be based on the invariant characteristics.

The rate of strain tensor has three functionally independent characteristics which can be taken as its eigenvalues $\lambda_i$ describing deformation rate intensity. The principal directions of the tensor are always mutually orthogonal providing a natural basis for the problem.

Vorticity, which characterizes locally a solid-body rotation, is actually a vector and has a unique invariant in itself, its length. Consideration of vorticity and strain tensor in a cojoint 3-dimensional space yields two other invariants, angles specifying orientation of vorticity vector relative to the basis prescribed by the strain velocity tensor. Thus we have six invariants in total.

If we decide to distinguish different kinds of flow merely by different colors, we then have only two degrees of freedom: the color tone and its brightness.

Therefore our suggestion is to abandon vorticity and to concentrate only on deformations. This forces us to retrieve the key information on deformations from two parameters that must be constructed as combinations of the strain velocity tensor eigenvalues.

Of three principal directions for the rate of strain tensor we single out those two meeting the requirement of maximum $(\max\{\lambda_1, \lambda_2, \lambda_3\})$ and minimum $(\min\{\lambda_1, \lambda_2, \lambda_3\})$ rates of deformation. Then we single out the subspace spanned by these two principal directions and designate this as a principal plane. The difference $\max\{\lambda_1, \lambda_2, \lambda_3\} - \min\{\lambda_1, \lambda_2, \lambda_3\}$ characterizes the degree of non-uniformity of deformation in this principal plane. Then we define the first parameter $D_1$ further referred to as the deformation index, as a certain ratio of this measure of non-uniformity to the relative velocity of volume change at any given point.

$$D_1 = \frac{\max\{\lambda_1, \lambda_2, \lambda_3\} - \min\{\lambda_1, \lambda_2, \lambda_3\}}{\lambda_1 + \lambda_2 + \lambda_3}. \tag{2}$$

This index serves as a quantitative measure for distinguishing different types of deformation in the principal plane irrespective of their intensity. The typical values of $D_1$ and corresponding kinds of deformation are presented in Table 1. Recall that all deformations are determined here without regard to vorticity. This means that all kinds of deformations with an accuracy to solid-body rotation are equivalent ones, as for instance, simple shear and pure shear.

**Table 1** Deformation index $D_1$ specific values [see definition (2)]

| $\lambda_i$ | Type of deformation | $D_1$ |
|---|---|---|
| $\lambda_1 < 0$, $\lvert\lambda_2\rvert \approx \lvert\lambda_3\rvert$ $\lvert\lambda_1\rvert \gg \{\lvert\lambda_2\rvert, \lvert\lambda_3\rvert, \lvert\lambda_2 + \lambda_3\rvert\}$ | 1-Dimensional compression (shock-wave discontinuity) | $\approx -1$ |
| $\lambda_1 > 0$, $\lvert\lambda_2\rvert \approx \lvert\lambda_3\rvert$ $\lambda_1 \gg \{\lvert\lambda_2\rvert, \lvert\lambda_3\rvert, \lvert\lambda_2 + \lambda_3\rvert\}$ | 1-Dimensional extension (1-dimensional rarefaction wave) | $\approx 1$ |
| $\{\lambda_1, \lambda_2\} < 0$ $\{\lvert\lambda_1\rvert, \lvert\lambda_2\rvert\} \gg \lvert\lambda_3\rvert$, $\lambda_1 \approx \lambda_2$ | Uniform 2-dimensional compression | $\approx -0.5$ |
| $\{\lambda_1, \lambda_2\} > 0$ $\{\lambda_1, \lambda_2\} \gg \lvert\lambda_3\rvert$, $\lambda_1 \approx \lambda_2$ | Uniform 2-dimensional extension | $\approx 0.5$ |
| $\{\lambda_1, \lambda_2\} < 0$, $\lambda_3 > 0$ $\lvert\lambda_1\rvert \approx \lvert\lambda_2\rvert \approx \lambda_3$ | Uniform compression in two directions and extension in a third one | $\approx -2$ |
| $\{\lambda_1, \lambda_2\} > 0$, $\lambda_3 < 0$ $\lambda_1 \approx \lambda_2 \approx \lvert\lambda_3\rvert$ | Uniform extension in two directions and compression in a third one | $\approx 2$ |
| $\lambda_1 \approx \lambda_2 \approx \lambda_3 \neq 0$ | Uniform overall compression or expansion | $\approx 0$ |
| $\lambda_1 + \lambda_2 + \lambda_3 \approx 0$ particularly, $\lambda_1 \approx -\lambda_2$, $\lambda_3 \approx 0$ | Isochoric deformation including isochoric plane deformation (pure shear, tangential discontinuity) | $\approx \pm\infty(\lvert D_1\rvert \gg 1)$ |

As is seen from the Table 1, one can easily distinguish between the shock-like and tangential discontinuities. To differentiate strong and weak jumps we determine an additional parameter, the second deformation index

$$D_2 = \max\{|\lambda_1|, |\lambda_2|, |\lambda_3|\}, \tag{3}$$

which specifies the intensity of deformation irrespective of type of deformation.

For visualization of flow patterns each type of deformation is assigned different color. We associate basic colors of RGB palette with the specific values of deformation index: $D_1 = 1$ – red, $D_1 = 0$ – green, and $D_1 = -1$ – blue (Fig. 1). Other intermediate values of $D_1$ are represented by a mixture of these prime colors. The Gaussian functions

$$r(D_1) = e^{-a(D_1-1)^2},\ g(D_1) = e^{-aD_1^2},\ b(D_1) = e^{-a(D_1+1)^2}, \tag{4}$$

with the inverse width $a = 1$ provide a good fitting of the hue intensities. The final hue intensity is determined by using index $D_2$ as follows

$$\begin{aligned} R(D_1, D_2) &= (1 - r(D_1)) \cdot (1 - D_2/\max(D_2)) + r(D_1),\\ G(D_1, D_2) &= (1 - g(D_1)) \cdot (1 - D_2/\max(D_2)) + g(D_1),\\ B(D_1, D_2) &= (1 - b(D_1)) \cdot (1 - D_2/\max(D_2)) + b(D_1). \end{aligned} \tag{5}$$

Here $\max(D_2)$ is the maximum value of index $D_2$ in the whole computational domain.

Depending on the numeric value of $D_1$ we can obtain from (4) either a pure basic color $\{r, g, b\}$ or a new color as a result of composition of basic colors (Fig. 1). Namely, in the case $|D_1| \lesssim 1/3\sqrt{a}$ or $|D_1 \pm 1| \lesssim 1/3\sqrt{a}$ we have one of three basic colors, while in the gaps between these intervals we have either the basic color or a mixture of two adjacent basic colors. For example, the value $D_1 = 0.5$ typical for the areas of 2-dimensional expansion gives the yellow pixel as a mixture of red and green while the contribution of the blue color vanishes [see Eq. (4)]. Finally, when $|D_1| \gg 1$ all these three basic colors $\{r, g, b\}$ mix in almost equal shares which should produce black color.

Subject to the parameter $D_2$ the resulting color $\{R, G, B\}$ can either remain unchanged or be inverted [Eq. (5)]. In the areas of weak deformation $[D_2 \ll \max(D_2)]$ the black or dark-gray hues transform to white or light-gray ones ($\{R, G, B\} \to 1$). However one cannot speak about an opposite transformation of the white tone $\{r, g, b\}$ to the black one $\{R, G, B\}$ because the combination $(r = g = b = 1)$ is not possible for any $D_1$. The color box in Fig. 2 (left plot) illustrates distribution of colors for different pairs $(D_1, D_2)$.

The use of formulae (4), (5) does not exclude a possibility of applying of other specific filters in concordance with the aims of the specific problem. For example, instead of the Gaussian functions in (4) one can use the roof functions and instead of the quasi-linear color modification via $D_2$ according to (5) one can apply the smooth relations like hyperbolic tangent.

Of the three tensor eigenvalues one can compose no more than three functionally independent invariant values. Index $D_1$ contains information on deformations in the principal plane but says nothing about the deformation in the orthogonal direction. If one wishes to describe deformation in this third, complement, direction, the set of invariants should be supplemented by a third invariant which could be determined by analogy with $D_1$ but in reliance on the third still not used mediate $\lambda_i$

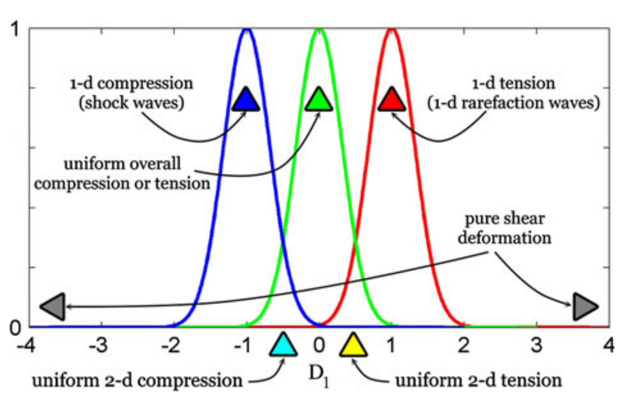


**Fig. 1** Association of different types of deformations and relevant discontinuities with RGB-palette

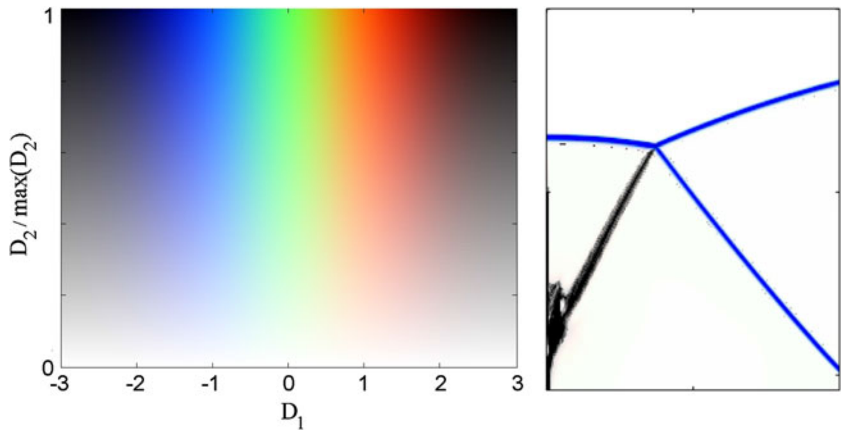


**Fig. 2** *Left plot* Distribution of colors for different combinations ($D_1$, $D_2$). *Right plot* Shock fronts (*blue*) and tangential discontinuity (*dark gray*) formed after a primary shock reflection from a flat surface (*left margin*)

$$D_1' = \frac{\max\{\lambda_1, \lambda_2, \lambda_3\} - \mathrm{mid}\{\lambda_1, \lambda_2, \lambda_3\}}{\lambda_1 + \lambda_2 + \lambda_3}, \tag{6}$$

where

$$\mathrm{mid}\{\lambda_1, \lambda_2, \lambda_3\} = \sum_{\mathrm{i}=1}^{3} \lambda_{\mathrm{i}} - \max\{\lambda_1, \lambda_2, \lambda_3\} - \min\{\lambda_1, \lambda_2, \lambda_3\}. \tag{7}$$

However, as we see further it is more convenient to design the relative value equivalent to eccentricity

$$D_3 = \frac{\max\{\lambda_1, \lambda_2, \lambda_3\} - \mathrm{mid}\{\lambda_1, \lambda_2, \lambda_3\}}{\max\{\lambda_1, \lambda_2, \lambda_3\} - \min\{\lambda_1, \lambda_2, \lambda_3\}}. \tag{8}$$

By definition $D_3$ assumes values in the range between 0 and 1. It appears as a measure of anisotropy of local deformation in the plane orthogonal to the principal direction corresponding to the maximum eigenvalue. Index $D_3$ proves to be useful in visualization of incompressible flows where $D_1$ and $D_1'$ degenerate becoming infinite. Without regard to $D_3$ the whole flow field should be colored in gray tone whose intensity depends on $D_2$. In this case, to analyze incompressible flows one can associate the color palette with parameter $D_3$.

In case of incompressible flow the relation between all three eigenvalues can be parameterized by the unique value $\alpha$

$$\lambda_1 = \lambda, \quad \lambda_2 = (\alpha - 1/2)\lambda, \quad \lambda_3 = (-\alpha - 1/2)\lambda, \tag{9}$$

where $\alpha = (-\infty, +\infty)$, and $\lambda$ is an arbitrary non-zero quantity. It is easy to show that transformations

$$\alpha \to -\alpha \tag{10}$$

and

$$\alpha \to \frac{2\alpha + 3}{4\alpha - 2} \tag{11}$$

convert the set of eigenvalues to themselves within the accuracy of relabeling eigenvalues or their synchronous rescaling which does not affect $D_3$. This means that consideration of the interval [0,3/2] is quite sufficient. The transformation (11) maps this interval [0,3/2] into the interval $[3/2, \infty)$, and then (10) spreads the positive-definite semiinfinite interval on the whole number axis. Figure 3 illustrates the dependence of $D_3$ on $\alpha$. The singled out values for $D_3$ are 0, 1/2 and 1, whose physical meaning is explained in Table 2.

In case of compressible flows one cannot use both $D_1$ and $D_3$ simultaneously with $D_2$ because we are limited by the drawing tools to only two degrees of freedom—the color and intensity. Index $D_1$ proves to be the most informative parameter since it allows identification of the basic types of jumps or smooth deformations. At the same time, it allows identification of tangential discontinuities both in the compressible

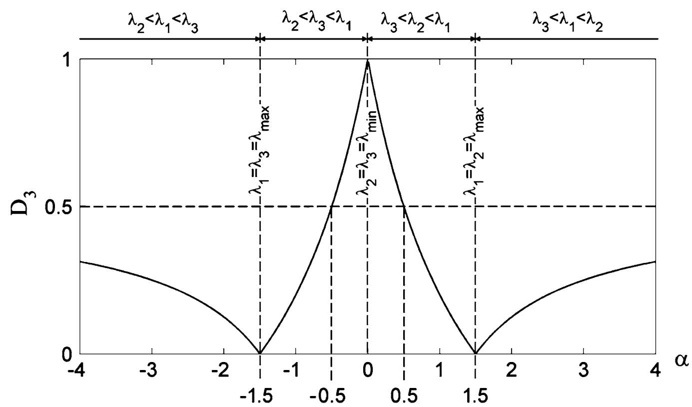


**Fig. 3** The dependence of $D_3$ on α-parameter

**Table 2** Deformation index $D_3$ specific values [see definition (8)]

| $\lambda_i$ | α | Type of deformation | $D_3$ |
|---|---|---|---|
| $\lambda_1 = \lambda_3 = -\frac{1}{2}\lambda_2$ | $\alpha = -3/2$ | 2-Dimensional extension, | 0 |
| $\lambda_1 = \lambda_2 = -\frac{1}{2}\lambda_3$ | $\alpha = 3/2$ | 1-Dimensional compression (Fig. 4a) | |
| $\lambda_1 = -\lambda_2,\ \lambda_3 = 0$ | $\alpha = -1/2$ | Plane isochoric deformation, | 1/2 |
| $\lambda_1 = -\lambda_3,\ \lambda_2 = 0$ | $\alpha = 1/2$ | e.g. tangential discontinuity (Fig. 4c) | |
| $\lambda_1 = 0,\ \lambda_3 = -\lambda_2$ | $\alpha = \pm\infty$ | | |
| $\lambda_2 = \lambda_3 = -\frac{1}{2}\lambda_2$ | $\alpha = 0$ | 1-Dimensional extension, | 1 |
| | | 2-Dimensional compression (Fig. 4b) | |

and incompressible flows. In the former case they are depicted by gray tones or by black color depending on $D_2$: in the latter case one can bind tangential jump to some specific color for $D_3 = 1/2$. Thus, the procedure of visualization developed by us covers all kinds of flat deformations irrespective of the kind of flow. Its advantage becomes apparent in that it is based on invariant characteristics that makes it applicable to arbitrary computational grids.

## 3 Numerical examples

The right plot in Fig. 2 demonstrates a simple example of discontinuities extraction from the velocity field which is obtained from computational simulation of a spherical shock reflection from a flat surface. Three-wave interaction of initial shock, reflected shock and a Mach stem form a Y-shape shock configuration with a weak flocculent shear discontinuity in the post-shock domain.

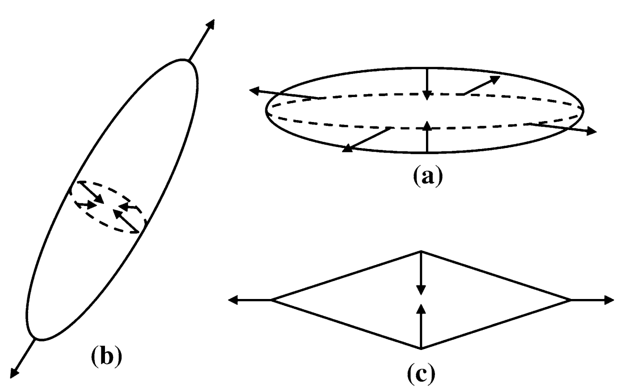


**Fig. 4** Different kinds of deformations in incompressible flow: **a** flattening, **b** stretching, **c** isochoric plane deformation (pure shear strain, tangential discontinuity)

The method developed becomes most effective when applied to the problems of complex gasdynamic flows with multiple discontinuities. One of these is the problem of a blast wave propagation in a non-uniform medium with multiple small-scale non-homogeneities of density. Such a problem can be met with in astrophysics of multi-phase interstellar medium segregated into small dense cloudlets and rarefied intercloud gas (Ostriker and McKee 1988).

The results of numerical simulation of supernova remnant evolution (Korolev 2006) are presented in Fig. 5 as a sequence of states of a blast wave produced by a supernova explosion. At early stages of supernova remnant expansion its inner regions are colored in green, which corresponds to uniform dilatation (Fig. 5, top-left). After first encounters with clouds the interaction between primary shock and clouds produces a multitude of secondary shocks (blue curves) and tangential discontinuities (black lines), and the riot of colors grows up (Fig. 5, top-right and bottom-left). Fauvist-like (Bowness et al. 1979) patterns of early stages of expansion gradually transit to pastel tones of the final stage when the shock wave decelerates and motion decays (Fig. 5, bottom-right). Please see the accompanying animation (Online Resource 1).

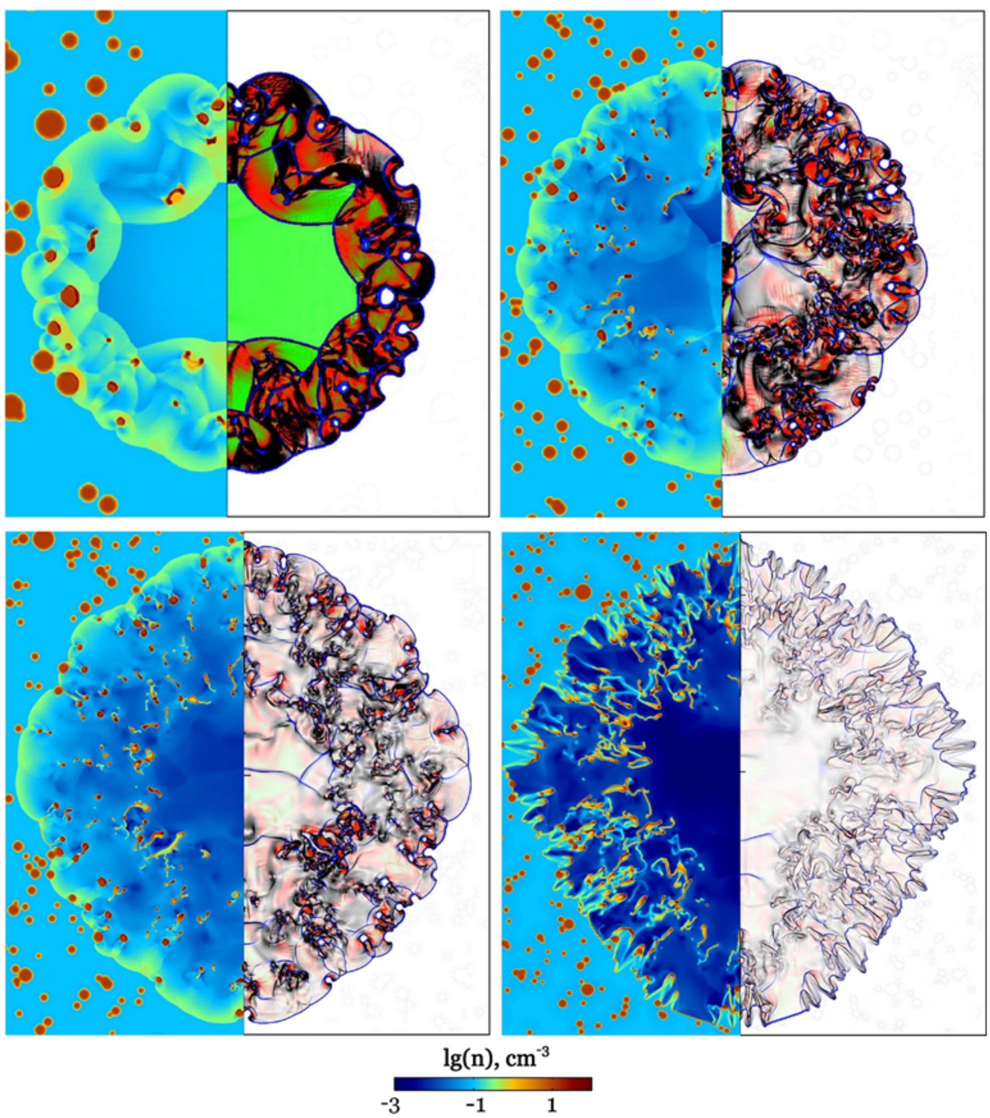


**Fig. 5** Supernova remnant evolution in a cloudy medium: *top-left* age $13 \times 10^3$ years, radius $\sim 25$ pc; *top-right* age $52 \times 10^3$ years, radius $\sim 40$ pc; *bottom-left* age $114 \times 10^3$ years, radius $\sim 50$ pc; *bottom-right* age $350 \times 10^3$ years, radius $\sim 60$ pc. Left half of each plot shows the gas density distribution while color-maps of deformation index $D_1$ are shown on the right half. The density scale is equal for all images while the spatial scale is lengthening

**Acknowledgments** The authors thank anonymous referees for their helpful remarks.

## References

Bowness A et al (1979) Post-impressionism. Cross-currents in European painting. Royal Academy of Arts & Weidenfeld and Nikolson, London

Korolev VV (2006) Large-scale non-linear processes in interstellar medium. Dissertation. Volgograd State University. Russian Federation

Ostriker JP, McKee CF (1988) Astrophysical blastwaves. Rev Mod Phys.60.1–68. doi:10.1103/RevModPhys.60.1

Vorozhtsov EV, Yanenko NN (1980) On some algorithms for shock wave recognition by shockcapturing computational results. Comput Fluids 8:313–326